RESPONSE TO REVIEWERS

Note: The reviewer's original comments are indicated in black, and our responses are indicated in blue. Figures in the manuscript are numbered and labeled using Arabic numerals, e.g., Figure 1; those in the response to reviewers file are numbered and labeled using Arabic numerals with a prefix "R", e. g. Figure R1.

Reviewer #1

Summary:

Based on the MITgcm LLC4320 data, this paper investigates the interaction between semidiurnal internal tide (SIT) and an anticyclonic eddy (AE) in the northern South China Sea. Through calculating the energy budget of the first three modes of SIT, the authors analyze the interaction between the modal SIT and AE. Results indicate that the AE can modulate the intensity and propagation of SIT.

Comments:

1. L13, As the authors have pointed out that the energy is transferred from SIT to AE, the value of the transferring rate (-3.0 mW m^-2) should be changed to 3.0 mW m^-2.

Responses: Thank you for this suggestion, the negative symbol has been removed from this sentence.

2. L77-79, "The model can effectively simulate free propagating internal waves such as ITs, while regional models cannot because of …". I disagree.

Responses: We apologize for using such an improper statement. We are trying to convey that current regional circulation models rarely consider the influence of far-field internal waves (IWs) on the near-field IWs when modeling IWs, because the open boundary condition in the SINGLE RUN case cannot introduce the forcing of low-mode IWs from the external region. A multi-layer nesting strategy, however, can make the regional circulation model include the effect of far-field IWs from the external region. The reviewer is right that the regional circulation model does have such abilities, although its implementation is complex and computationally

demanding. Now we rewrite this sentence as "The model can effectively simulate free-propagating internal waves such as ITs, while regional models get weaker IWs in the simulated region when they do not introduce forcing of low-mode IWs from the external region."

3. L109-110, I do not understand why model decomposition is related to horizontal resolution.

Responses: We are sorry for this information gap, the dispersion relation of linear IWs is:

$$k_z = \sqrt{\frac{N^2-\omega^2}{N^2-f^2}}k_h \text{ , or } \lambda_\mathrm{h} = \sqrt{\frac{N^2-\omega^2}{N^2-f^2}}\lambda_\mathrm{z} \qquad \text{（R1）}$$

for IWs at a fixed frequency ω, the horizontal wavelength λ_h is proportion to the vertical wavelength λ_z, and hence inversely proportional to the mode number. When the horizontal wavelength of the mode-n internal tide is less than two times the horizontal resolution of model ($\lambda_n^h < 2\Delta x$), the mode-n internal tide cannot be identified. As a result, the mode decomposition is related to both the vertical resolution and horizontal resolution.

4. L117 and Figure 1, The regionally averaged barotropic tidal currents do not make sense, because the phases of tidal currents at different points are different.

Responses: We agree with the reviewer that the phase of barotropic tide varies spatially. However, from Figure R1, we can see that the mean value of the phase velocity of the semidiurnal barotropic tide in the region R2 is more than 100 m s^{-1} (which can be estimated using $c = \sqrt{gH}$ with a mean water depth of 2000 m), and the corresponding horizontal wavelength is more than 6000 km. The zonal distance of region R2 is about 300 km, meaning that the phase change of semidiurnal barotropic tide could be ignored in region R2.

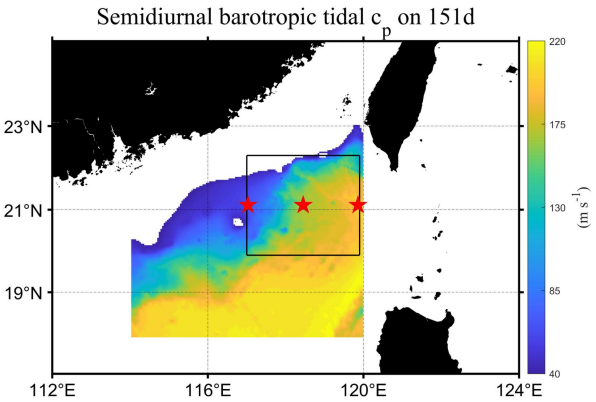

Figure R1 Spatial distribution of the phase velocity of semidiurnal barotropic tide in the study area, with the three red pentagrams indicating the stations analyzed in Figure R2.

It can be seen clearly from Figure R2 that the phase difference of the zonal velocity of semidiurnal barotropic tide is small, even at different stations. It is reasonable that spatial averaging in a relatively small region does not departure the real results significantly. Moreover, Figure 1b-c are just used for qualitative examination of the spring tidal moment.

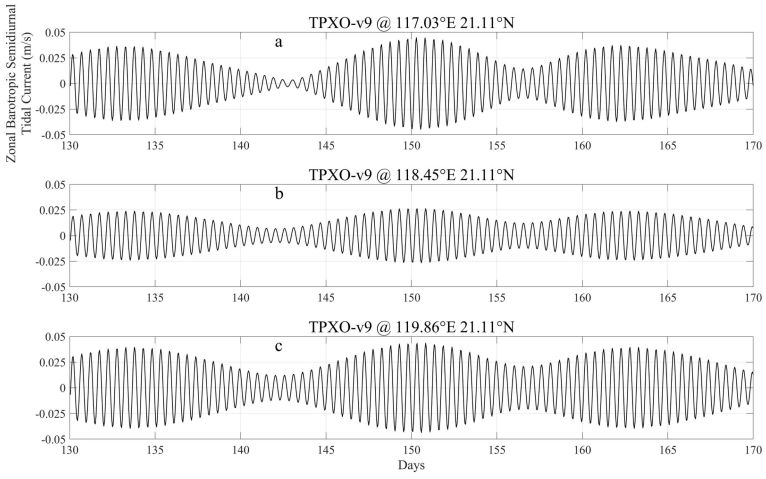

Figure R2 Zonal velocity of semidiurnal barotropic tide for the three stations marked with red pentagram in Figure R1. Data are from the TPXO-v9 model, using the TMD toolkit.

5. L135, Please introduce how to calculate the HKE and APE.

Responses: We apologize for this gap, the method (Kelly et al., 2012) calculating HKE and APE is:

$$\mathrm{HKE}_n = \frac{\rho_0 H}{2}(u_n^2 + v_n^2) \qquad (R2)$$

$$\mathrm{APE}_n = \frac{\rho_0 H}{2}\left[\left(1 - \frac{f^2}{\omega^2}\right)\frac{p_n^2}{c_n^2}\right] \qquad (R3)$$

Reference:

Kelly, S. M., Nash, J. D., Martini, K. I., Alford, M. H., and Kunze, E. (2012). The cascade of tidal energy from low to high modes on a continental slope. Journal of physical oceanography, 42(7), 1217-1232.

6. L163-165, The authors use the theoretical estimation of Vic et al. and L_1 of Xu et al. to demonstrate that the simulated mode-2 SIT is consistent with the theory (Figure 3). However, it seems that the simulated mode-1 SIT (Figure 2) is not consistent with L_1 of Xu et al. Moreover, it seems that the calculated L_3 (L178) is not consistent with the result shown in Figure 4.

Responses: We are sorry for this confusion, the estimates of propagation distance based only on empirical equation may have a bias, instead, we calculated the SIT's energy fluxes directly throughout the whole SCS (at depths greater than 200 m) using LLC4320 output. Take day 151 as an example in Figure R3. The propagation distance of mode-1 SIT exceeds 1000 km, which is consistent with the L_1 of Xu et al. (2016). The propagation distance of mode-2 SIT is about 400 km, which is larger than the result of empirical equation (125-188 km). Similarly, the propagation distance of the mode-3 SIT is about 80 km, also larger than the result of empirical equation. We acknowledge that the empirical equation $L_n \approx L_1/n^3$ can reflect the propagation distance decreasing with the increasing mode number qualitatively, but its quantitative estimation of the propagation distance is less precise.

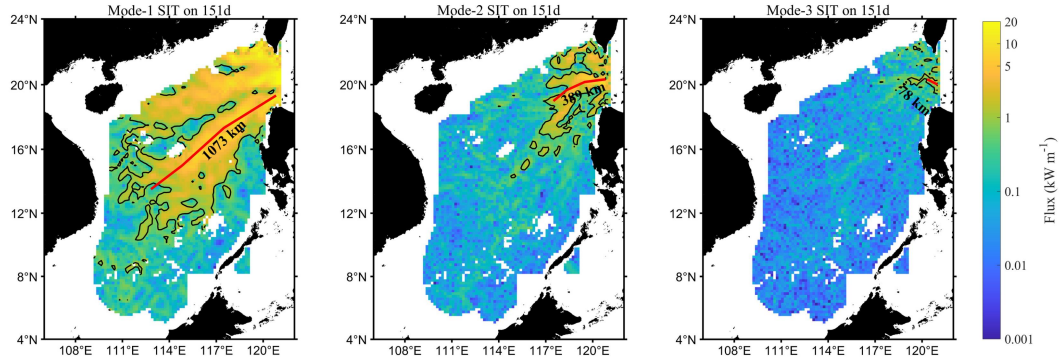

Figure R3 Spatial distribution of energy flux for the first three modes of SITs in the SCS.

Reference:

Xu, Z., Liu, K., Yin, B., Zhao, Z., Wang, Y., and Li, Q. (2016). Long-range propagation and associated variability of internal tides in the South China Sea. Journal of Geophysical Research: Oceans, 121(11), 82688286.

7. Figure 6. If the IT is locally generated, the corresponding conversion from barotropic tides (C_0x, x=1,2,3,…) should be positive. If the local IT is influenced by that propagated from remote source, the value of conversion might be negative. It is generally recognized that high-mode IT cannot propagate a long distance from the source. To be specific, high-mode IT (especially mode-4 and mode-5) generated at the Luzon Strait might not reach the study region. Therefore, how to explain the negative values of C_04 and C_05?

Responses: we thank the reviewer for this valuable comment. First, C_{0n} is examined by comparing with depth-integrated energy conversion from barotropic tide to all baroclinic modes E_{bt2bc} (calculated by Equation R5). It is found that the spatial distribution of $\sum_{n=1}^{5} C_{0n}$ (Figure R4a) is nearly the same as that of E_{bt2bc} (Figure R4b), which indicates a reliable calculating of C_{0n}.

$$C_{0n} = -\nabla H \cdot \boldsymbol{u_0}(p_n \phi_n)|_{z=-H} \qquad (R4)$$

$$E_{bt2bc} = g \int_{-H}^{\eta} \rho' w_{bt} dz \qquad (R5)$$

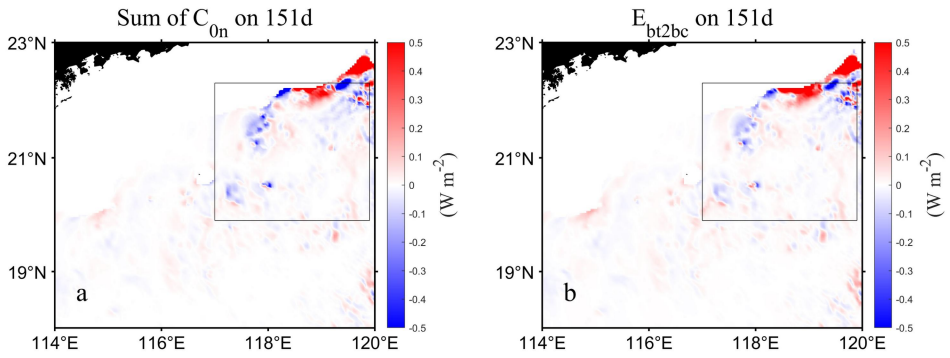

Figure R4 (a-b) Spatial distribution of barotropic to baroclinic energy conversion rates on day 151 in the northern SCS, calculated using Equations R4 and R5, respectively.

Second, the positive or negative of the barotropic to baroclinic energy conversion rate in Equation R4 is determined by topographic gradient, barotropic velocity, and bottom pressure perturbation (Zilberman et al., 2009), i.e., the meridional component of C_{0n}^{y}:

$$C_{0n}^{y} = -\frac{dH}{dy}\hat{p}_n\hat{v}_{bt}cos(\theta_p - \theta_v) \qquad \text{(R6)}$$

where $\hat{p}_n$ and θ_p are the amplitude and Greenwich phase of bottom pressure perturbation for nth mode, and $\hat{v}_{bt}$ and θ_v are the amplitude and Greenwich phase of meridional barotropic velocity, respectively. We calculated the conversion rate from barotropic tide to mode-4 baroclinic tide C_{04} (for the northern region of R2 only, where negative values occur) using Equation R6. Figure R5 shows that C_{04} is mainly regulated by its meridional component C_{04}^{y}, since the meridional topographic gradient is essentially positive at depths from 250 to 2000 m, the positive or negative of conversion rate is shaped by the cosine of the phase difference $(\Delta\theta = \theta_p - \theta_v)$, which is negative near the 250-500 m isobath at 22°N (Figure R5d), resulting in that C_{04} is predominantly negative in the northern region of R2.

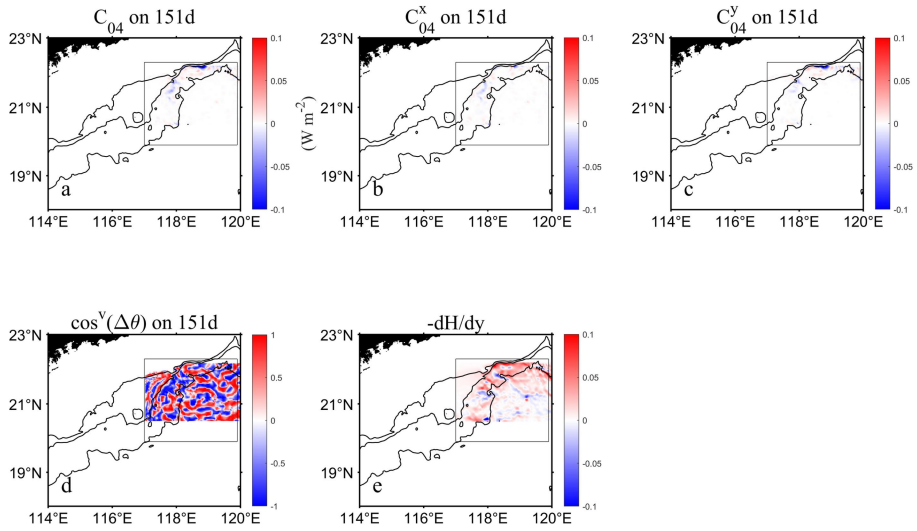

Figure R5 (a-c) Spatial distribution of the conversion rate from barotropic tide to mode-4 baroclinic tide C_{04}, as well as its zonal component C_{04}^{x} and meridional component C_{04}^{y} on day 151, (d) cosine of the phase difference between bottom pressure perturbation and meridional barotropic velocity, and (e) meridional topographic gradient with three isobaths of 250 m, 500 m, and 2000 m, respectively.

At last, we examine the northward energy fluxes of the first five modes of SITs in the region R2 (Figure R6), and find that when the mode-1 SIT propagates toward the northern SCS (Figure R6a), mode 1 transmits higher-mode SITs over subcritical continental slope (Figure R6b-e), i.e., the region between the magenta contour and the 2000 m isobath. Wang et al. (2018) demonstrate that the subcritical shelves are more conducive to the occurrence of transmission of higher-mode internal tides. Based on the direction of energy fluxes (Figure R6d-e), it can be seen that the transmitted mode-4 and mode-5 SITs propagate northward, whereas the locally-generated mode-4 and mode-5 SITs propagate southward, which are in the opposite directions, leading to the negative values of C_{04} and C_{05} in this region. Negative values of the conversion rate indicate that the internal tide energy is transferred to the barotropic tide through pressure work, which is not involved in turbulent kinetic energy dissipation. In addition, negative conversion rates have been seen in some studies, e.g., Figure 5 of

Song and Chen (2020), Figure 6 of Wang et al. (2016), and Figure 9 of Xu et al. (2016).

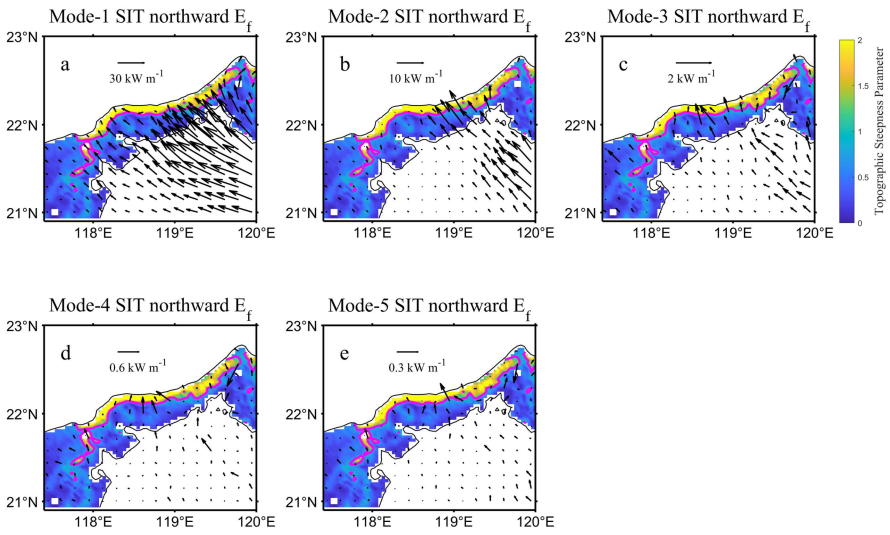

Figure R6 Spatial distribution of the northward component (incident wave) of the energy flux (arrows) for the first five SITs modes on day 151, superimposed on the contour map of topographic steepness parameters from 250 to 2000 m, with magenta contour for $\gamma = 1$.

References:

Song, P., and Chen, X. (2020). Investigation of the internal tides in the Northwest Pacific Ocean considering the background circulation and stratification. Journal of Physical Oceanography, 50(11), 3165-3188.

Wang, S., Chen, X., Li, Q., Wang, J., Meng, J., and Zhao, M. (2018). Scattering of low-mode internal tides at different shaped continental shelves. Continental Shelf Research, 169, 17-24.

Wang, X., Peng, S., Liu, Z., Huang, R. X., Qian, Y. K., and Li, Y. (2016). Tidal mixing in the South China Sea: An estimate based on the internal tide energetics. Journal of Physical Oceanography, 46(1), 107-124.

Xu, Z., Liu, K., Yin, B., Zhao, Z., Wang, Y., and Li, Q. (2016). Long-range propagation and associated variability of internal tides in the South China Sea. Journal of Geophysical Research: Oceans, 121(11), 82688286.

Zilberman, N. V., Becker, J. M., Merrifield, M. A., and Carter, G. S. (2009). Model estimates of M_2 internal tide generation over Mid-Atlantic Ridge topography. Journal of Physical Oceanography, 39(10), 2635-2651.

8. Section 3.2.1 and corresponding content in section 3.1.1, The authors find that the calculated r_E is different from the theoretical r_E for mode-2 SIT and speculate that it is caused by the interference of SIT after a reflection at the continental slope. Hence, they analyze the reflection of mode-2 SIT in section 3.2.1. I have several questions for this analysis. First, if mode-2 SIT is reflected at the slope, mode-1 and mode-3 SITs are also reflected at the slope. Why only mode-2 SIT causes interference as well as a r_E different from the theoretical value? Second, as shown in Figure 11, the incoming and reflected energy fluxes are in different directions, how to form interference in this case?

Responses: we thank the reviewer for this valuable comment. We decompose the incident and reflected energy fluxes of mode-1 and mode-3 SITs (Figure R7 and Figure R8). Figure R7 and Figure R8 share a similar pattern for mode 1 and mode 3, indicating that energy reflection occurs when the incident SITs encounter the continental slope, which confirms that topographic reflection exists in different modes. However, it is difficult to directly judge the presence or absence of reflection from the direction of mode-1 energy flux, which is not referred to in the manuscript.

There are two reasons why the r_E is different from theoretical value. One is topographic reflection of lower mode SITs, the other is interference between transmitted (onshore, Figure R6c) and locally-generated (offshore) higher mode SITs. The combined effect of reflection and transmission leads to a deviation from the theoretical values of r_E for the first three modes, with the absolute errors being 9%, 16%, and 18% on day 151.

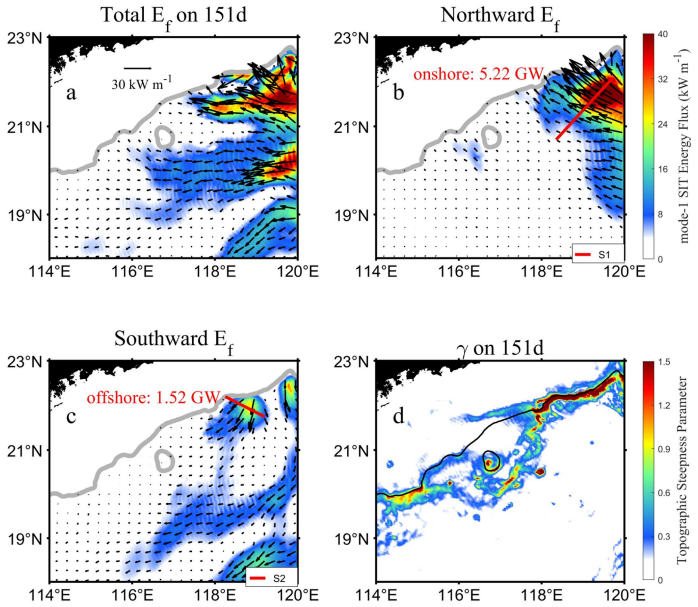

Figure R7 The energy flux of mode-1 SIT on day 151 in (a), (b), and (c) for total, northward, and southward, respectively. The energy fluxes integrated along sections S1 and S2 are labelled as onshore and offshore values, respectively. The topographic steepness parameter for SIT on day 151 is presented in (d).

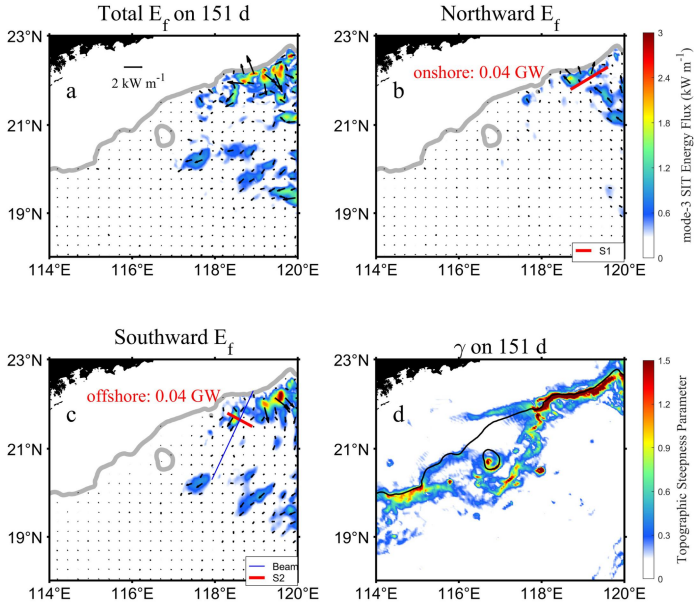

Figure R8 Same as Figure R7, but for the mode 3.

9. Figure 11a, Compared with previous studies (e.g. Kerry et al., 2013; Xu et al., 2021), the energy flux pattern of SIT shown in this study is odd.

Responses: We are sorry for this confusion. For the energy flux of mode-1 SIT in Figure R7a, it is generally in agreement with those of the earlier studies, e.g., Zhao (2014). The energy flux bifurcates around (119.5°E, 21.0°N) when the Kuroshio loop is present, as indicated in both Kerry et al. (2013) and Xu et al. (2021)'s work. The incoming energy fluxes at the continental slope reported by Kerry et al. (2013) and Xu et al. (2021) are the total value of all modes, with magnitudes up to 40 kW m^{-1} and 25 kW m^{-1}, respectively. Our result of incoming energy fluxes of mode-2 SIT is 15 kW m^{-1}, among which the maximum of the reflected part is 8 kW m^{-1}, in this way, the reflection of mode-2 SIT is difficult to observe in Kerry et al. (2013) and Xu et al. (2021)'s results.

References:

Kerry, C. G., Powell, B. S., and Carter, G. S. (2013). Effects of remote generation sites on model estimates of M_2 internal tides in the Philippine Sea. Journal of Physical Oceanography, 43(1), 187-204.

Xu, Z., Wang, Y., Liu, Z., McWilliams, J. C., and Gan, J. (2021). Insight into the dynamics of the radiating internal tide associated with the Kuroshio Current. Journal of Geophysical Research: Oceans, 126(6), e2020JC017018.

Zhao, Z. (2014). Internal tide radiation from the Luzon Strait. Journal of Geophysical Research: Oceans, 119(8), 5434-5448.

10. L322-326, The authors find that the reflected mode-2 SIT on day 151 is larger than that on day 137, and then conclude that the AE promotes the reflection of SIT. This is imprecise, because the incoming SIT is also increased from day 137 to 151 (section 3.1.1).

Responses: We thank the reviewer for this valuable comment. As the reviewer pointed out, the incident mode-2 SIT on day 151 (0.70 GW) is larger than that on day 137 (0.31 GW), and more internal tide energy is reflected on day 151 (0.31 GW) than

on day 137 (0.10 GW). Meanwhile, we compare the reflection coefficient (i.e., the reflected energy divided by the incident energy), which is 32% on day 137 and increases to 44% on day 151, increasing by 12% under the influence of an anticyclonic eddy (on day 151), implying that the eddy promotes a reflection of mode-2 SIT. We added this in the manuscript.

11. L347, There is no c^U in Equation (6).

Responses: We correct this spelling error. It should be c_n^U.

12. L350, There is no c in Equation (7).

Responses: We correct this spelling error. It should be c_{n}.